PLASMA FEATURES IN A MEDIUM-POWER ARCJET

HIROKAZU TAHARA*, KAZUHITO KOMIKO**, LULU ZHANG**,
KEN-ICHI ONOE+ and TAKAO YOSHIKAWA++

Abstract

Spectroscopic measurement was carried out to understand the arc structure and the flowfield in a 10-kW-class water-cooled steady-state nitrogen arcjet. In the expansion nozzle, the pressure and electron density drastically decreased downstream, and therefore the plasma was in thermodynamical non-equilibrium although the plasma in the constrictor was expected to be nearly in a temperature-equilibrium condition. The radial profiles of the physical properties for N_2 and N_2^+ showed that there existed a core flow with high vibrational and rotational temperatures and great electron number densities on the center axis even at the nozzle exit. Both temperatures on the arcjet axis at the nozzle exit increased linearly with the input power regardless of mass flow rate as well as the electron temperature in the constrictor. The characteristic lines covered temperature ranges from 6,000 to 10,000 K for the vibrational temperature in input power levels of 5-11 kW and from 500 to 2,000 K for the rotational temperature. Furthermore, arcjet flowfields were numerically analyzed using a quasi-one dimensional core-flow model, in which radial mass transfer, and dissociation and ionization processes in thermal and chemical non-equilibrium condition are considered. The analyzed results are compared with the experimental ones.

Introduction

The medium-power arcjet thruster is a promising device suitable for future missions for planetary exploration and construction of large stations. The recent research and development of arcjet thrusters encounter significant problems as follows: (1) low thrust efficiency; (2) severe electrode erosion. These features are related to the arc structure and the flowfield in the arcjet chamber. However, inner plasma properties are not clear because of the complicated flowfield including the interaction between arc and gas flow, energy transfer and internal energy excitations of atoms and molecules etc[1]-[5].

In a previous study, we examined plasma properties in an arcjet discharge chamber with an expansion nozzle by means of optical diagnostics in order to understand the arc structure and the thermodynamical non-equilibrium flowfield[1]-[6]. Electron densities and several temperatures such as molecular vibrational and rotational ones were measured although they were horizontally-integrated average values, i.e. not functions of radial position, because of no Abel transformations as mentioned in detail later[3],[5]. In this study, we examine radial profiles of the physical properties since the radially-dependent values are very important because of understanding of radial structure of the arcjet flowfield.

This paper describes a study to understand quantitatively physical properties in a 10-kW-class steady-state direct-current arcjet engine, particularly thermodynamical non-equilibrium nitrogen flowfields in the expansion nozzle, by means of optical diagnostics and numerical analysis. Spectroscopic measurement is carried out, and several plasma properties are examined from the data. Atomic electron excitation, molecular vibrational and rotational temperatures are determined, and electron densities are also estimated using hydrogen $H\beta$

* Associate Professor, Faculty of Engineering Science, Osaka University, 1-3, Machikaneyama, Toyonaka, Osaka 560, Japan.
** Graduate Student of Osaka University.
+ Research Associate, Osaka University.
++ Professor, Osaka University.

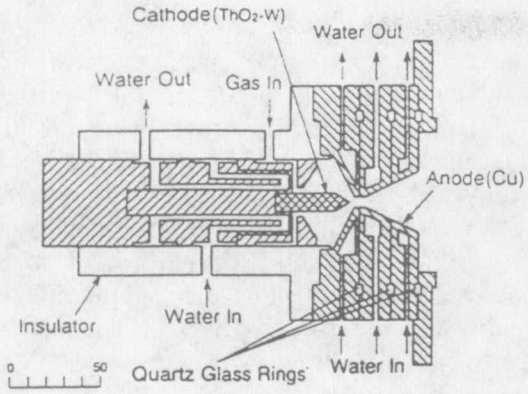

(a) Configuration of arcjet.

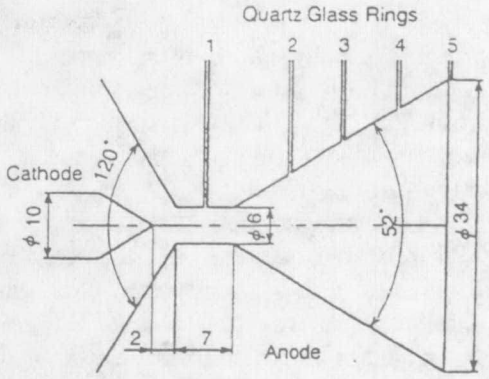

(b) Arrangement of electrodes and quartz glass rings.

Fig.1 Cross section of 10-kW-class water-cooled steady-state arcjet. The expansion nozzle is exchanged to another one with quartz glass rings in different axial positions for optical measurement.

line Stark broadening with a mixture of nitrogen and a few percent seed hydrogen. Their radial profiles are determined using Abel transformations except for the determination of electron density. Furthermore, arcjet flowfields are numerically analyzed using a quasi-one dimensional core-flow model, in which radial mass transfer, and dissociation and ionization processes in thermal and chemical non-equilibrium (partially-LTE) condition are considered[4],[6]. The analyzed results are compared with the experimental ones.

Experimental Apparatus

Figure 1 shows the cross section of the 10-kW-class steady-state arcjet used for this study. The electrodes are of water-cooled. A constrictor has a diameter of 6 mm and a length of 7 mm. A divergent nozzle has an exit diameter of 34 mm and an angle of 52 deg. The ratio of the cross sectional area of the nozzle exit to that of the constrictor is 32.1. The convergent-divergent anode made of copper was divided into the expansion nozzle part and the constrictor-plenum-chamber part, and both anode parts were electrically insulated from each other with a silicon sheet; thus, the current entering each anode part could be measured[1],[2]. As shown in Fig.1(b), the anode is provided with quartz glass rings for arc observation and optical diagnostics. A cylindrical cathode made of 2-%-thoriated tungsten has a diameter of 10 mm. The gap between the electrodes, which is defined as the axial distance between the cathode tip and the constrictor upstream exit, is set to 2 mm. Nitrogen is used as working gas. The gas is injected tangentially from the upstream end of the discharge chamber. Pressures were measured with a manometer at various locations in the arcjet[1]-[3],[5]. Also, temperatures of cooling water were measured, and the thermal efficiency was estimated[1]-[6].

The arcjet is operated with input power levels of 3-12 kW at discharge currents of 70-150 A. High-frequency discharge of 3 MHz and amplitude 2 kV is used for arc initiation. The arcjet is set on a flange of a vacuum tank, into which the heated gas is exhausted, as shown in Fig.2. The vacuum tank 0.8 m in diameter and 1.5 m long is evacuated to 1-10 Pa during

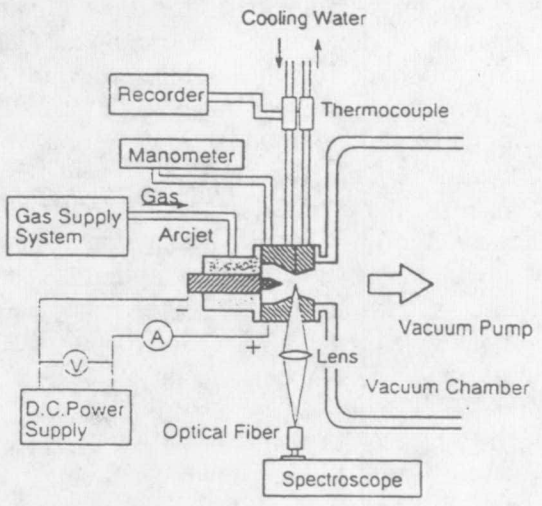

Fig.2 Experimental system of arcjet on flange of vacuum tank.

operations.

Emission spectroscopic measurement is conducted as reliable plasma diagnostics in arcjet chambers. Light comes from the plasma through a quartz glass slit of 0.5 mm in width, as shown in Fig.1(b). The emission is collected by a lens of 80 mm in focal length and is introduced into a 0.5-m monochrometer through an optical fiber. The monochrometer of diffraction-grating-type HAMAMATSU C5095 is provided with 150 and 2,400 grooves/mm grating plates and a 1024-channel diode array detector, achieving spectral resolutions of 0.8 and 0.05 nm, respectively, per detector channel. Electron number densities and several plasma temperatures of an atomic excitation temperature for N^+ and molecular vibrational and rotational temperatures for N_2 and N_2^+ are determined using the spectral data. The electron density is estimated from the Stark width of hydrogen Hβ line 486.1 nm, in which a mixture of nitrogen and a few percent seed hydrogen is used.

The spectral intensities measured in this experiment are line-of-sight values, measured by looking through the arc from the side perpendicular to the center line of the arcjet. For line-of-sight measurements, the intensity values correspond to horizontally-integrated values of intensity as a function of position, and we simply calculated horizontally-average physical properties from them as presented in Refs. [3] and [5]. However, since the radially-dependent values are very important because of understanding of radial arc structure, the radially-dependent emission coefficient is determined from the measured spectral intensities using well-known Abel transformations except for the determination of electron density.

The atomic-ion excitation temperature is determined using a relative intensity method of spectral lines, i.e., by means of Boltzmann plotting with N II spectral lines of 417.6, 444.7, 453.0, 460.7, 461.4, 462.1, 463.1, 566.7, 567.6 and 568.0 nm as shown in Fig.3(a) under the assumption of local thermodynamical equilibrium (LTE), in which the linearity of the Boltzmann plotting and the theoretical limiting criteria on electron density and local pressure were considered for estimation of separation from LTE[5],[7]. We call the atomic-ion excitation temperature the electron temperature because the atomic-ion excitation temperature is considered to be almost equal to the temperature of free electrons in plasmas under LTE conditions. The molecular vibrational temperature is also determined from an intensity ratio of two lower energy transitions as well as the determination of the atomic-ion excitation temperature under the assumption of partial LTE, in which LTE was not satisfied completely[5],[8]. Spectral band heads of 380.4 and 375.4 nm (second positive band $C^3\Pi_u$-$B^3\Pi_g$) for N_2 and of 427.8 and 423.6 nm (first negative band $B^2\Sigma_u^+$-$X^2\Sigma_g^+$) for N_2^+ are used[9],[10], as shown in Figs.3(b) and 3(c).

The relative intensity method can not be

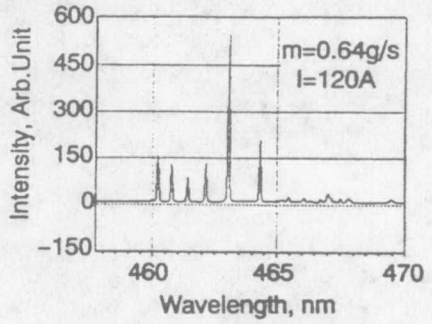

(a) N^+ spectral lines.

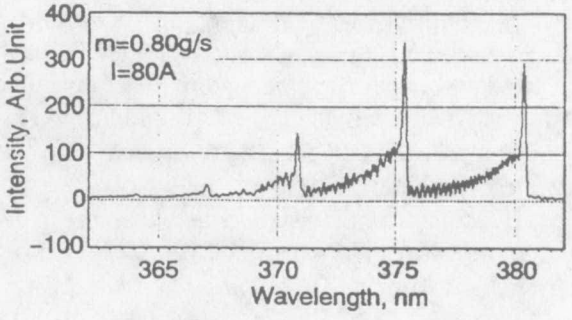

(b) N_2 second positive bands.

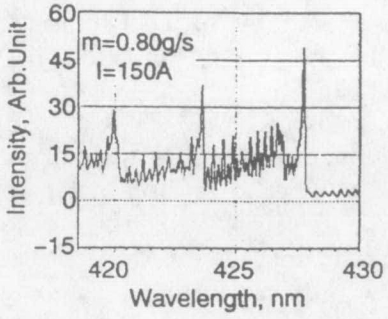

(c) N_2^+ first negative bands.

Fig.3 Typical narrow spectra emitted from plasma in arcjet discharge chamber.

used to determine rotational temperatures because the rotational lines are too close together and overlapped. Therefore, in general the theoretical intensity distribution for a band is calculated with an assumed rotational temperature and compared to the measured spectrum[11],[12]. The horizontally-integrated average rotational temperature, not radially-dependent rotational temperature, was found iteratively by varying the temperature of the theoretical distribution[3],[5]. The transition bands of N_2 $C^3\Pi_u$-$B^3\Pi_g$ at 380.4 nm and of N_2^+ $B^2\Sigma_u^+$-$X^2\Sigma_g^+$ at 427.8 nm were used. However, in order to simply calculate radial profiles of rotational temperatures in the present study, after Abel tranformations of measured emission intensities at 380.0 and 379.0 nm in the N_2 $C^3\Pi_u$-$B^3\Pi_g$ band (band head 380.4 nm) or at 427.0 and 425.5 nm in the N_2^+ $B^2\Sigma_u^+$-$X^2\Sigma_g^+$ band (band head 427.8 nm), the ratio of their two intensities at a same radial position is compared to a theoretical intensity ratio with an assumed rotational temperature.

Experimental Results and Discussion

Operating Characteristics and Plasma Features in Constrictor

The characteristics of the discharge voltage vs discharge current and the pressure in the constrictor vs input power were shown in Refs.[1]-[3],[5][6]. The discharge voltage gradually decreased with the discharge current at a constant mass flow rate, and it was approaching a constant value for high current levels above 120 A. An increase in the mass flow rate raised the voltage with a constant current. Thus, the electrical input power ranged from 3 to 11 kW. Also, the thermal efficiency evaluated was 50 to 70 % for all operations. The pressure in the constrictor increased linearly with the input power at each mass flow rate and ranged from 10 to 30 kPa. Furthermore, the measured current fraction on the anode showed that most of the discharge current entered the expansion nozzle part regardless of operational conditions. It was expected that the arc passed through the constrictor and attached to the expansion nozzle, which was called a constricted arc.

For the spectra emitted from the plasma in the constrictor, as shown in Refs.[1]-[3],[5],[6], the bands for N_2 and N_2^+ were observed at low discharge currents around 100 A or at small mass flow rates around 0.2 g/s, i.e., in low power operations below about 5 kW. On the other hand, the atomic ion spectra N II were observed at higher discharge currents or at larger mass flow rates.

Figure 4 shows the radial profiles of the atomic-ion N^+ excitation temperature, i.e., the electron temperature and the N_2^+ vibrational temperature in the constrictor. The vibrational temperature could be evaluated in low input power levels below 5 kW and the electron temperature in higher power levels. Both temperatures have peaks on the center axis, and

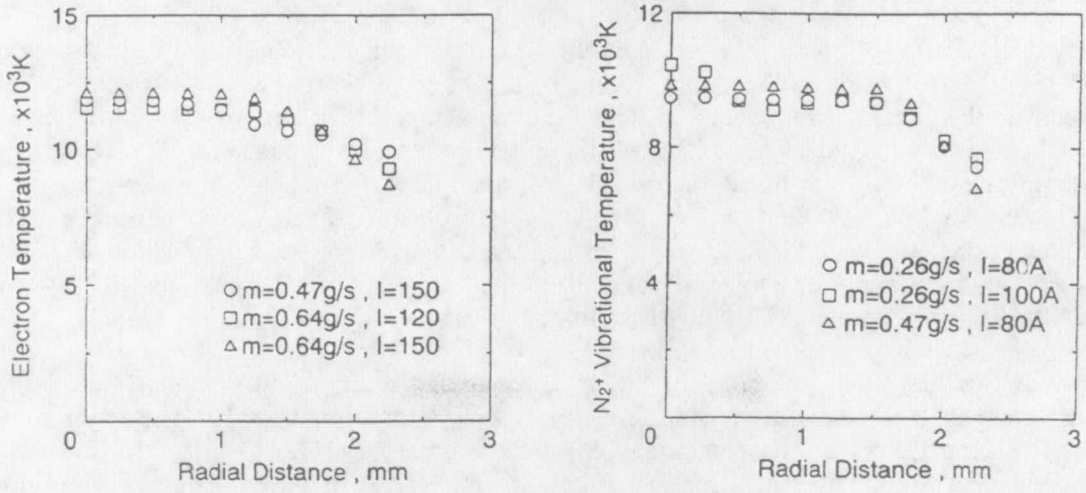

(a) Electron temperature. (b) N_2^+ vibrational temperature.

Fig.4 Radial profiles of electron temperature and N_2^+ vibrational temperature in constrictor.

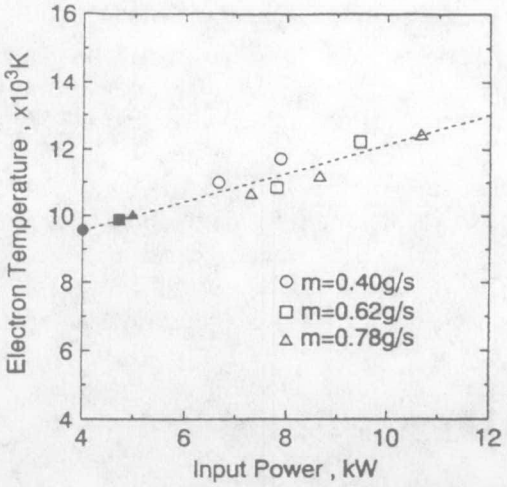

Fig.5 Dependence of input power on peak electron temperature on arcjet centerline in constrictor. The electron temperatures inferred by extrapolation of the characteristic line are represented with closed symbols.

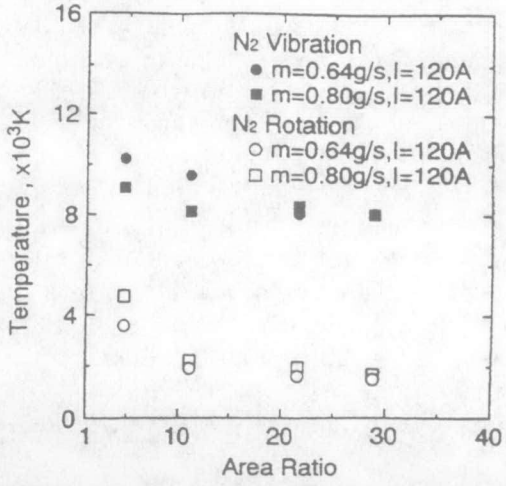

Fig.6 Axial variations of vibrational and rotational temperatures of N_2 on arcjet centerline in expansion nozzle after Abel transformations. The area ratio is defined as the ratio of the axial-plane cross sectional area of the expansion nozzle to that of the constrictor.

they are about 12,000 and 10,000 K for the electron temperature and the vibrational one, respectively. Both temperatures decrease radial-outward although their profiles are almost flat within 1-1.5 mm in diameter. An increase in the mass flow rate raises the peak temperature on the centerline at the same discharge current and brings about a great decrease near the tail. This is a so-called thermal pinch effect[5]. As shown in Fig.5, the peak electron temperature on the axis increases linearly with the input power, and the characteristic line is independent of the mass flow rate. When we infer electron temperatures around 4-5 kW, which could not be evaluated in this optical measurement, by extrapolation of the characteristic line, they are about 10,000 K as shown with closed symbols in Fig.5. The inferred electron temperatures almost equal the N_2^+ vibrational temperatures near the center axis as shown in Fig.4(b); that is, the plasmas in the constrictor are expected to be nearly in temperature equilibrium conditions. Also, the horizontally-integrated average electron density in the constrictor ranged from 1×10^{15} to 3×10^{16} cm^{-3} in input power levels of 6-11 kW.

Non-Equilibrium Plasmas in Expansion Nozzle

As shown in Refs. [3] and [5], the pressure on the discharge chamber wall decreased drastically from 10-30 kPa in the constrictor to the order of 10^2 Pa downstream in the nozzle because of supersonic expansion. This feature agreed with that of the horizontally-integrated average electron density; that is, the electron density reached the order of 10^{13} cm^{-3} at the nozzle exit. As a result, no atomic ion spectrum was observed in the expansion nozzle, and the bands of N_2 and N_2^+ were mainly observed. This was expected because excitation collisions between atomic ions and electrons hardly occurred under the low pressure and small electron density environment in the nozzle. Hence, the heated gas was expected to be in high non-equilibrium throughout the nozzle.

Figure 6 shows the axial variations of the vibrational and rotational temperatures of N_2 on the center line in the expansion nozzle after Abel transformations. The vibrational temperature is almost kept a constant value of about 8,000-9,000 K. This is because of much slower relaxation of vibrational excitation modes than the characteristic flow time[13],[14]. On the other hand, the rotational temperature is considered to drastically decrease near the inlet in the nozzle, i.e. from the downstream exit of the constrictor to an

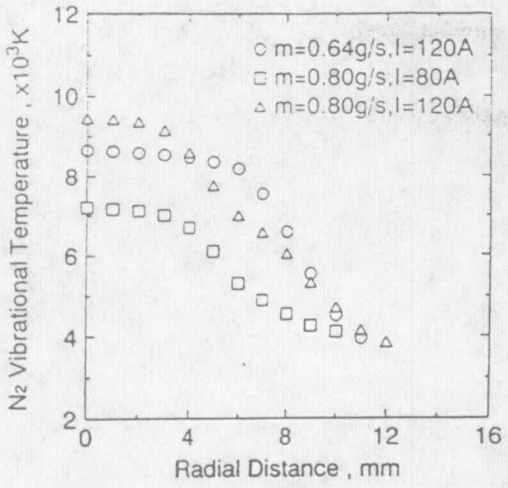

(a) N_2 vibrational temperature.

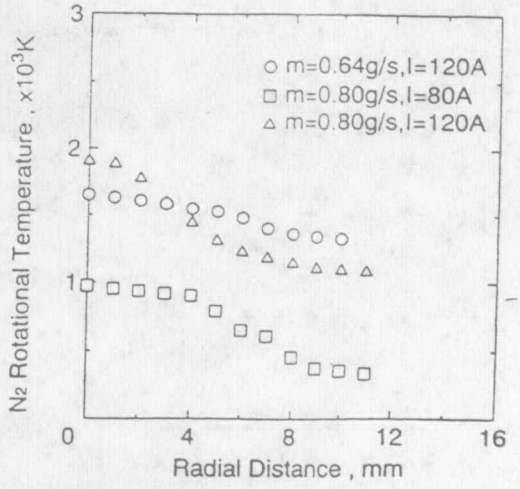

(b) N_2 rotational temperature.

Fig.7 Radial profiles of vibrational and rotational temperatures of N_2 at expansion nozzle exit.

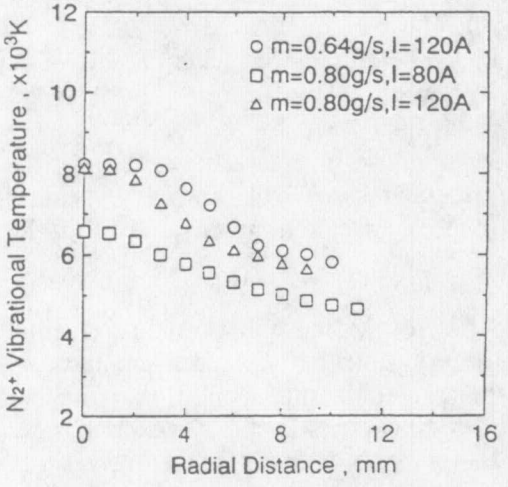

(a) N_2^+ vibrational temperature.

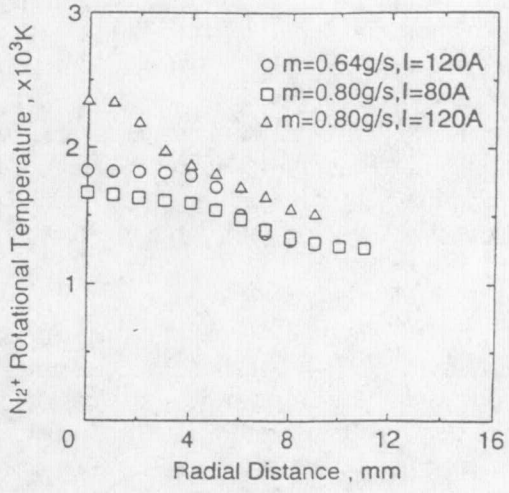

(b) N_2^+ rotational temperature.

Fig.8 Radial profiles of vibrational and rotational temperatures of N_2^+ at expansion nozzle exit.

area ratio of about 10, since the rotational temperature is expected to be about 10,000 K because of near-temperature-equilibrium in the constrictor, and then it is kept about 2,000 K downstream. These features on the axial variations are reasonable compared with analytical results with a quasi-one dimensional non-equilibrium flow model, as shown later[4],[6].

Figures 7 and 8 show the radial profiles of the vibrational and rotational temperatures for N_2 and N_2^+, respectively, at the expansion nozzle outlet. Four temperatures have peaks on the centerline as well as those in the constrictor, and there are high temperature

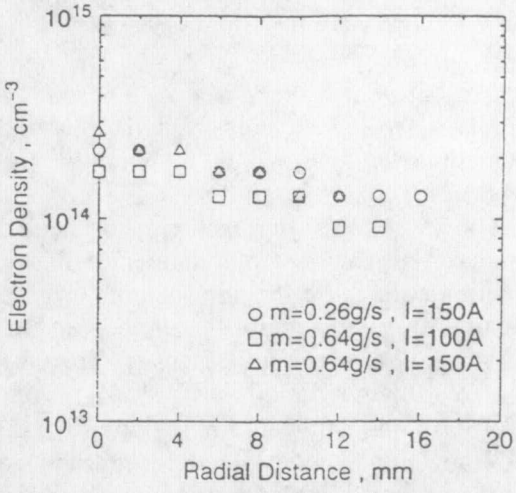

Fig.9 Radial profiles of horizontally-integrated average electron density at nozzle exit without Abel transformations.

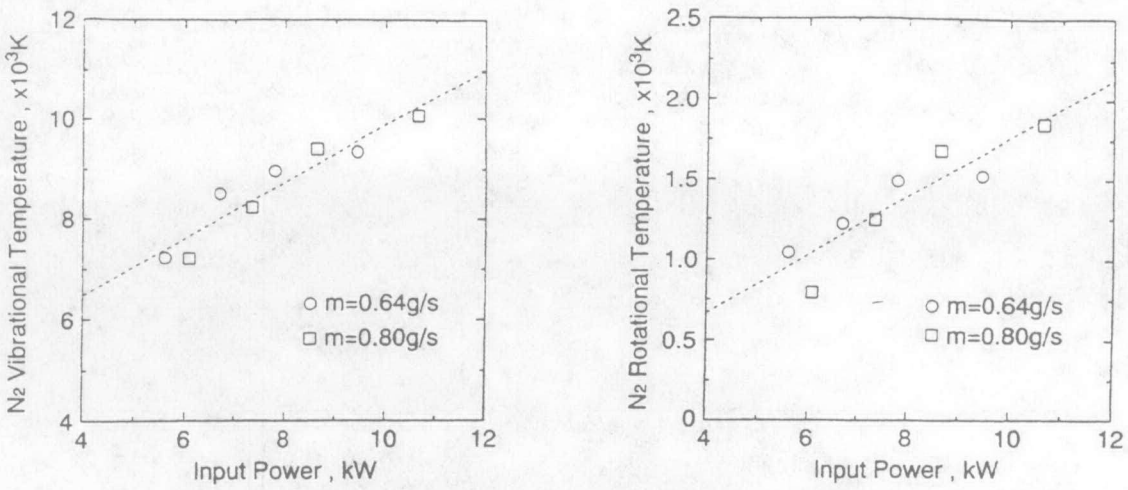

(a) N_2 vibrational temperature. (b) N_2 rotational temperature.

Fig.10 Dependence of input power on peak vibrational and rotational temperatures of N_2 on arcjet centerline at expansion nozzle exit after Abel transformations.

regions within 4–6 mm in diameter. The peak temperatures increase with the mass flow rate at a constant current of 120 A except for the N_2^+ vibrational temperature, and the profiles become sharper. On the other hand, the temperatures, particularly the rotational temperatures, gradually decrease radial–outward at a low discharge current of 80 A or at a low mass flow rate of 0.64 g/s compared with those at 120 A with 0.80 g/s. As shown in Fig.9, the horizontally–integrated average electron density also has a peak of $2–4\times10^{14}$ cm^{-3} on the arcjet centerline at the nozzle exit. These features show that there exist core flows with high temperatures and large number densities on the center axis even at the nozzle exit.

Figure 10 shows the dependence of the input power on the vibrational and rotational temperatures of N_2 on the arcjet axis at the nozzle exit. Both temperatures increase linearly with the input power regardless of mass flow rate in this operational condition range as well as the electron temperature in the constrictor. The characteristic lines cover temperature ranges from 6,000 to 10,000 K for the vibrational temperature in input power levels of 5–11 kW and from 500 to 2,000 K for the rotational temperature.

Flowfield Analysis

Modeling of Arc–Heated Flowfield

The present analysis is carried out using a quasi–one dimensional core–flow model[15],[16]. An arc–heated flowfield is divided into two regions; one is a current conduction region, i.e., arc column on the center line of the arcjet, and the other is a cold gas flow region surrounding the arc column. We assume for simplification of calculation as follows: (1) the temperature in the cold flow region is constant, and it equals the wall temperature; (2) the temperatures of heavy species, electron and vibration are considered; (3) the temperature in the arc column region is radially uniform and axially variable; (4) the pressures in both regions balance, and they are radially uniform and axially variable; (5) axial heat transfer and viscosity are neglected; (6) axial gas flow is considered in both regions although radial mass transfer is implicitly considered; (7) current density is radially uniform in the arc column region; (8) dissociation is considered for nitrogen molecules, and first ionization is considered for nitrogen atoms and molecules, and (9) electrical input power is not dissipated into bremsstrahlung and heat conduction loss to the wall.

Governing Equations and Boundary Conditions

The equations of mass, momentum and energy conservations in partially-LTE condition are described in detail in Refs.[2]-[4]. The boundary conditions at the inlet, i.e., in the axial position of the cathode tip are determined from previous experimental results[1],[2] of temperatures, pressures, arc radii as described in Refs. [2] and [4]. Another boundary condition is required for determination of all physical quantities at the upstream boundary. The ratio of mass flow rates in the dual flow is an iterative parameter as explained later.

In thermal and chemical non-equilibrium flowfield analysis, the following reactions are considered[17]: $N_2 + M_i = 2N + M_i$ (M_i: N_2, N_2^+, N, N^+, e)

$$N + e = N^+ + 2e$$
$$N + N = N_2^+ + e$$
$$N_2 + N^+ = N_2^+ + N$$
$$N_2 + e = N_2^+ + 2e$$

In the energy equations, the energy exchanges of translation-vibration, translation-electron, rotation-electron and electron-vibration are considered[13],[18]. The harmonic oscillator model is employed for the vibrational energy.

Method of Numerical Simulation

The closed equations are solved computationally; that is, the variables are integrated in the downstream direction from the cathode tip to the arc attachment point where the radius of the arc column equals the wall radius. In this calculation, the gradients of the physical quantities are frozen just near the sonic point to avoid its singularity, and the subsonic flow is connected smoothly with the supersonic one.

Solving the basic equations for a set of the inlet parameters with an arbitrary ratio of mass flow rates in the arc column and cold gas region, the arcs for N_2 do not attach to the anode, even to the expansion nozzle, although the arcs for Ar attached to the constrictor wall. Thus, a series of the numerical integration for N_2 is carried out for variation of the ratio of mass flow rates at the upstream boundary until the Mach number of the cold gas flow reaches unity at the downstream exit of the constrictor and a real solution is determined by the supersonic expansion condition. Also, we assume that Joule heating does not occur downstream from the constrictor outlet.

Calculation Results and Discussion

The electrode shape with a constrictor of 6 mm in diameter and 7 mm long and an electrode gap of 2 mm, which equals that for the above experimental arcjet, is used for the present calculation. The discharge current is 150 A, and the nitrogen mass flow rate is varied.

The axial variations of the arc column radius in thermal and chemical non-equilibrium condition for N_2 are shown in Fig.11. The arcs pass through the constrictor and do not attach even to the expansion nozzle. We may need to improve the interface conditions between the arc column and cold gas flow region in the present analytical model. An increase in the mass flow rate decreases the arc radius at a same

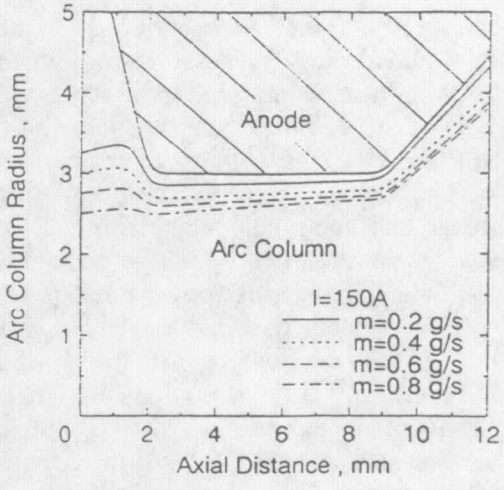

Fig.11 Calculated axial variations of arc column radius in constrictor.

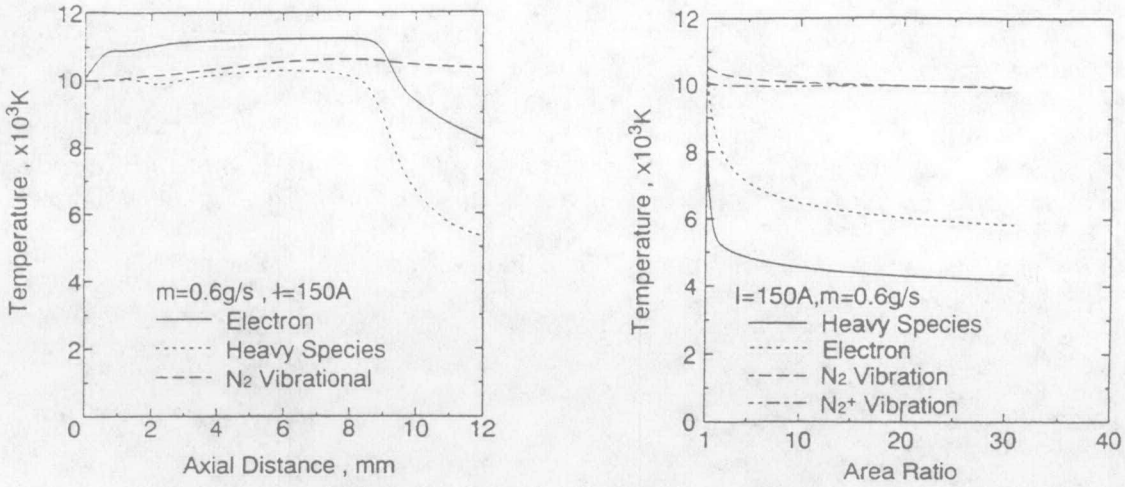

(a) In constrictor. (b) In expansion nozzle.

Fig.12 Calculated axial variations of temperatures of electron, heavy species and vibration in nitrogen arcjet chamber.

axial position; i.e., thermal pinch works effectively with a large mass flow rate. It is also noted that the arc shapes calculated in partially-LTE are almost equal to those in LTE as shown in Refs. [1] and [2].

The axial variations of the electron, heavy species and vibrational temperatures are shown in Fig.12. The electron temperature is little larger than the heavy species one in the plenum discharge chamber and constrictor in spite of the relatively high local pressure. They are kept about 11,000 and 10,000 K, respectively, in the constrictor. The vibrational temperature gradually increases from 10,000 to 10,500 K in the constrictor. An increase in the mass flow rate raises the heavy species temperature although it decreases the electron and vibrational temperatures. Therefore, it is approaching a thermodynamical equilibrium condition. In the expansion nozzle, as thermal energy is smoothly converted into kinetic energy, the heavy species temperature drastically decreases downstream compared the electron temperature. This is because of little energy transfer from heated electrons to heavy particles. The vibrational temperatures for N_2 and N_2^+ have small variations in the nozzle. These tendencies of the calculated temperatures agree with those of the experimental ones[1]-[3],[5],[6].

Conclusions

Spectroscopic measurement was conducted to understand the arc structure and the flowfield in a 10-kW-class water-cooled steady-state nitrogen arcjet. In the expansion nozzle, the pressure and electron density drastically decreased downstream, and therefore the plasma was in thermodynamical non-equilibrium although the plasma in the constrictor was expected to be nearly in a temperature-equilibrium condition. The radial profiles of the physical properties for N_2 and N_2^+ showed that there existed a core flow with high vibrational and rotational temperatures and great electron number densities on the center axis even at the nozzle exit. Both temperatures on the arcjet axis at the nozzle exit increased linearly with the input power regardless of mass flow rate as well as the electron temperature in the constrictor. The characteristic lines covered temperature ranges from 6,000 to 10,000 K for the vibrational temperature in input power levels of 5-11 kW and from 500 to 2,000 K for the rotational temperature. Furthermore, arcjet flowfields were numerically analyzed using a quasi-one dimensional core-flow model. The analyzed results showed that the arc for N_2 passed through the constrictor and that in the expansion nozzle the heavy species temperature drastically decreased downstream compared with the electron and vibrational temperatures. The calculated results agreed with the experimental ones.

References

1. H. Tahara, T. Sakakibara, K. Onoe and T. Yoshikawa," Discharge Characteristics and Inner Plasma Feature of a High-Power DC Arcjet Thruster," AIAA-90-2534, 1990.
2. H. Tahara, T. Sakakibara, K. Onoe and T. Yoshikawa," Experimental and Numerical Studies of a 10 kW Water-Cooled Arcjet Thruster," Proc. AIDAA/AIAA/DGLR/JSASS 22nd Int. Electric Propulsion Conf., Vol.1, Paper No. 91-015, 1991.
3. H. Tahara, N. Uda, K. Onoe, Y. Tsubakishita and T. Yoshikawa," Optical Measurement and Numerical Analysis of Medium-Power Arcjet Non-Equilibrium Flowfields," AIAA/AIDAA/DGLR/JSASS 23rd Int. Electric Propulsion Conf., Paper No. 93-133, 1993.
4. N. Uda, H. Tahara, K. Onoe and T. Yoshikawa," Flowfield Analysis of an Arcjet Thruster," Proc. 18th Int. Symp. Space Technology and Science, Vol.1, p.277, 1992.
5. H. Tahara, N. Uda, K. Onoe, Y. Tsubakishita and T. Yoshikawa," Discharge Features in a Steady-State Nitrogen Arcjet Engine with an Expansion Nozzle," IEEE Trans. Plasma Science, Vol.22, p.58, 1994.
6. K. Komiko, L. Zhang, K. Onoe, H. Tahara and T. Yoshikawa," Optical Measurement and Numerical Analysis of 10-kW-Class Steady-State Arcjet Flowfields," 19th Int. Symp. Space Technology and Science, Paper No. 94-a-51, 1994.
7. W.L. Wiese, M.W. Smith and B.M. Glennon, Atomic Transition Probabilities, U.S.GPO, Washington, 1963.
8. S. Ono and S. Teii," Vibrational Temperature in a Weakly Ionized Steady-State Nitrogen Discharge Plasma," J. Phys. D.: Appl. Phys., Vol.16, p.163, 1983.
9. R.W. Nicholls," Frank-Condon Factors to High Vibrational Quantum Numbers I: N_2 and N_2^+," J. Research of the National Bureau of Standards - A. Physics and Chemistry -, Vol.65A, p.451, 1961.
10. R.W.B. Pearse and A.G. Gaydon, The Identification of Molecular Spectra, 2nd Ed., New York: John Wiley & Sons, 1950.
11. G. Herzberg, Molecular Spectra and Molecular Structure, I. Spectra of Diatomic Molecules, New York: D. van Nostrand, 1959.
12. D.M. Phillips," Determination of Gas Temperature from Unresolved Bands in the Spectrum from a Nitrogen Discharge," J. Phys. D: Appl. Phys., Vol.8, p.507, 1975.
13. R. Matsuzaki," Quasi-One-Dimensional Aerodynamics with Chemical, Vibrational and Thermal Nonequilibrium," Trans. Japan Soc. Aero. Space Sci., Vol.30, p.243, 1988.
14. P. Sagnier and L. Marraffa," Parametric Study of Thermal and Chemical Nonequilibrium Nozzle Flow," AIAA-89-1856, 1989.
15. W. Herman, U. Kogelschatz, L. Niemeyer, K. Ragaller and E. Schade," Experimental and Theoretical Study of a Stationary High-Current Arc in a Supersonic Nozzle Flow," J. Phys. D., Vol.7, p.1703, 1974.
16. A. Sasoh," An Analytical Study on Positive Column in an Arcjet Thruster," AIAA-90-2564, 1990.
17. C. Park," On Convergence of Computation of Chemical Reacting Flows," AIAA-85-0247, 1985.
18. Y. Sakamura and M. Nishida," Viscous Shock Layer Analysis Using a Three-Temperature Model," Proc. 19th Int. Symp. Shock Waves, 1993.